HAL
open science

Targeted Radionuclide Therapy Decreases Melanoma Lung Invasion by Modifying Epithelial-Mesenchymal Transition-Like Mechanisms

Hussein Akil, Jacques Rouanet, Claire Viallard, Sophie Besse, Philippe Auzeloux, Jean-Michel J.-M. Chezal, Elisabeth Miot-Noirault, Mercédès Quintana, Françoise Degoul

To cite this version:

Hussein Akil, Jacques Rouanet, Claire Viallard, Sophie Besse, Philippe Auzeloux, et al.. Targeted Radionuclide Therapy Decreases Melanoma Lung Invasion by Modifying Epithelial-Mesenchymal Transition-Like Mechanisms. Translational Oncology, 2019, 12 (11), pp.1442-1452. 10.1016/j.tranon.2019.07.015 . hal-02343369

HAL Id: hal-02343369

https://hal.science/hal-02343369v1

Submitted on 2 Nov 2019

HAL is a multi-disciplinary open access archive for the deposit and dissemination of scientific research documents, whether they are published or not. The documents may come from teaching and research institutions in France or abroad, or from public or private research centers.

L'archive ouverte pluridisciplinaire **HAL**, est destinée au dépôt et à la diffusion de documents scientifiques de niveau recherche, publiés ou non, émanant des établissements d'enseignement et de recherche français ou étrangers, des laboratoires publics ou privés.

Translational Oncology
www.transonc.com

Volume 12 Number 11 November 2019 pp. 1442–1452 1442

Targeted Radionuclide Therapy Decreases Melanoma Lung Invasion by Modifying Epithelial-Mesenchymal Transition-Like Mechanisms☆

Hussein Akil*,*,1, Jacques Rouanet*,†,‡,1, Claire Viallard*, Sophie Besse*, Philippe Auzeloux*, Jean-Michel Chezal*, Elisabeth Miot-Noirault*, Mercedes Quintana* and Françoise Degoul[a]

*UMR 1240 INSERM, University of Clermont Auvergne, Clermont-Ferrand, France; †Department of Dermatology and Oncodermatology, CHU Estaing, Clermont-Ferrand, France; ‡Centre Jean Perrin, Clermont-Ferrand, France

Abstract

Melanin-radiolabeled molecules for targeted radionuclide therapy (TRT) provide a promising approach for the treatment of pigmented melanoma. Among these radiolabeled molecules, the iodinated melanin-specific binding molecule ([^{131}I]ICF01012) has shown a significant antitumor effect on metastatic melanoma preclinical models. We report herein that [^{131}I]ICF01012 decreases the epithelial-mesenshymal transition-like (EMT-like) markers in both *in vivo* and *in vitro* three-dimensional (3D) melanoma spheroid models. [^{131}I]ICF01012 spheroids irradiation resulted in reduced clonogenic capacity of all pigmented spheroids accompanied by increased protein expression levels of phosphorylated H2A.X, p53 and its downstream target p21. In addition, [^{131}I]ICF01012 treatment leads to a significant increase of cell pigmentation as demonstrated in SK-MEL3 human xenograft model. We also showed that [^{131}I]ICF01012 decreases the size and the number of melanoma lung colonies in the syngeneic murine B16BL6 *in vivo* model assessing its potentiality to kill circulating tumor cells. Taken together, these results indicate that [^{131}I]ICF01012 reduces metastatic capacity of melanoma cells presumably through EMT-like reduction and cell differentiation induction.

Translational Oncology (2019) 12, 1442–1452

Introduction

Melanoma, one of the deadliest forms of skin cancer, is a malignant tumor that arises from melanocytes, the pigment melanin-producing cells. Worldwide, approximately 80% of skin cancer-related deaths are due to melanoma, and unfortunately its incidence rate continues to increase [1]. Today, it is well known that malignant melanoma shows a high tendency to invade and metastasize. One of the fundamental processes of melanoma tumor progression and metastasis formation is a pseudo-like epithelial-mesenchymal transition (EMT-like) as melanocytes cannot be considered as epithelial cells. Indeed, EMT in cancer is frequently associated with poor prognosis. This genetic program promotes loss of epithelial and induction of mesenchymal phenotypes, enhancing tumor cells motility, invasion, and consequently the ability to disseminate to the metastatic sites [2]. Metastatic melanoma, treated with standard conventional chemotherapy, has been historically associated with poor outcomes. Currently, targeted therapy using specific small-molecule inhibitors against the RAS–RAF–MEK–ERK pathway, which is hyperactivated in more than 50% of melanomas (*i.e.* BRAF and MEK inhibitors) or immunotherapy using monoclonal antibodies against immune checkpoints (*i.e.* anti-CTLA4 and anti-PD-1/PD-L1) have shown remarkable clinical efficacy with a significant improvement of overall survival in patients with advanced or metastatic disease [3,4].

Address all correspondence to: Hussein Akil, UMR 1240 INSERM, University of Clermont Auvergne, Clermont-Ferrand, France. E-mail: hussein.akil@outlook.fr, jacques.rouanet@inserm.fr, claire.viallard@gmail.com, sophie.besse@inserm.fr, philippe.auzeloux@inserm.fr, j-michel.chezal@uca.fr, elisabeth.noirault@uca.fr, mercedes.quintana@inserm.fr, francoise.degoul@inserm.fr

Financial support: This work was supported by the Ligue Régionale Contre le Cancer (2015 and 2016). H. AKIL was supported by a fellowship from the Auvergne Regional council and the European Community. J. ROUANET is supported by a doctoral fellowship granted by the SFD (French Society for Dermatology).

[1]These authors contributed equally to this work.

Received 10 June 2019; Revised 17 July 2019; Accepted 18 July 2019

© 2019 The Authors. Published by Elsevier Inc. on behalf of Neoplasia Press, Inc. This is an open access article under the CC BY-NC-ND license (http://creativecommons.org/licenses/by-nc-nd/4.0/).

1936-5233/19
https://doi.org/10.1016/j.tranon.2019.07.015

However, recurrences due to the non- or short lasting-responses [5], and the serious autoimmune-related toxic effects induced by checkpoint inhibitors [6] remain major problems. Beside these therapies, radiotherapy is also proposed for the management of melanoma [7]. For many years, melanoma was thought to be a radioresistant tumor. Nevertheless, recent studies have demonstrated the effectiveness of external photon-beam radiotherapy in melanoma treatment such as stereotactic radiosurgery and/or radiotherapy for patients with brain or bone metastases [8]. One of the most important features of melanoma is the presence of melanin pigments. Two major types of melanin are synthesized in melanocytes: the black-brown melanin called eumelanin and the yellow-red one called pheomelanin. These pigments are produced and stored within specific membrane-enclosed lysosome-related organelles known as melanosomes [9,10]. Melanins are indeed present into cytoplasm of melanocytes, within melanosomes, but also in the extracellular space, as free "naked melanin" called melanocore [11]. It is worth mentioning that melanins can reduce response to radiotherapy and chemotherapy due to its scavenging capacity for reactive oxygen species and drugs [12]. It has also been described that eumelanin is predominantly expressed in primary lesions, whereas pheomelanin is associated to the disease progression [13]. Using ^{123}I-BZA2, a melanin radiolabeled benzamide derivative, it has been noted that about 45% of melanoma metastases are pigmented [14]. Thus, melanins provide a perfect target for melanoma-selective internal radionuclide therapy, mainly for advanced stage melanoma patients who have progressed after all current therapies. Three main approaches using directed radiolabeled agents to melanin or melanogenesis-related proteins have been developed: radioimmunotherapy, radiolabeled peptides, and radiolabeled small-molecules [15]. Radioimmunotherapy using β-emitting ^{188}Rhenium-monoclonal antibodies against the extracellular melanin has shown clinical efficacy in relatively small number of patients with advanced unresectable or metastatic melanoma [16]. Peptide analogues to α-MSH (α-melanocytes-stimulating hormone) targeting the MC1R (melanocortin-1 receptor) appears to be potentially useful for targeting melanoma [17]. Nonetheless, the heterogeneous expression level of MC1R and the considerable kidney uptake of these radiolabeled-peptide analogues limit this approach. Radiolabeled small-molecules, such as benzamide derivatives, are known to bind melanin pigment, which induces their selective accumulation in melanomas [18]. Indeed, Mier and colleagues have shown that ^{131}I-BA52, a radioiodinated benzamide, induces antitumor effects associated with more than 2-year survival rate in 3 of 5 treated patients with metastatic melanoma [19]. Our laboratory validated an ^{131}I-labeled quinoxaline derivative molecule, N-(2-(diethylamino) ethyl)-6-iodoquinoxaline-2-carboxamide dihydrochloride salt (ICF01012), for its melanin specificity, high uptake and retention in tumor cells, as well as its rapid clearance from non-target tissues and antitumoral efficacy using ^{123}I- ^{125}I-labeled and non-radiolabeled ICF01012 [20–24]. The use of different iodine isotopes allows characterization studies without modifying the quinoxaline structure. If molecular mechanisms by which External Beam Radiation Therapy (EBRT) modulates invasion in preclinical models are quite well described [25], there is no such data on the impact of TRT. In our previous studies, we showed that [^{131}I]ICF01012 reduces spontaneous lung metastases generated from subcutaneous primary B16BL6 tumor [21], and that could be associated to the anti-angiogenic effect of [^{131}I]ICF01012 [23].

Here, we extend our knowledge on the capacity of [^{131}I]ICF01012 to modify metastatic potential of melanoma both in *in vivo* and *in vitro,* 3D spheroid, cell culture models. Importantly, we showed that [^{131}I]ICF01012 significantly decreases the number and the size of lung colonies in B16BL6 murine model as well as the expression of pro-metastatic factor in both *in vivo* and *in vitro* models. Melanoma xenografts treatment with [^{131}I]ICF01012 increases the level of both eumelanin and pheomelanin pigments, suggesting a global effect of [^{131}I]ICF01012 on melanogenesis.

Materials and Methods

Cell Culture and Cell Lines

Murine B16BL6 melanoma cell line was obtained from the laboratory of Pr. Fidler (Houston, TX, USA). Murine B16F10, human SK-MEL3 and SK-MEL28 melanoma cell lines were purchased from the ATCC. SK-MEL28 cells were grown in MEM-Glutamax (Invitrogen) with 10% FCS (Eurobio) and 4 μg/μl gentamycin (Invitrogen). B16BL6, B16F10 and SK-MEL3 cell lines were cultured as described [24].

Animal Models

Female Swiss nu/nu mice and male C57BL/6 J (6 weeks old) were respectively purchased from JanvierLabs and Charles River Laboratories (France). All animal studies were carried out in accordance with the "Guide for the Care and Use of Laboratory Animals" and were approved by the local ethics committee (C2E2A) under the number: CE64–12.

Tumor Establishment and Radiotherapy Protocols

The murine syngeneic B16BL6 tumors and the human SK-MEL3 xenografts were established and treated with [^{131}I]ICF01012 as previously described [24].

Tumor Collection

For melanin assays, tumors were excised, frozen in N_2 and stored at −80 °C during the radioactive decay (80 days; 10 times a half-life of the iodine-131 isotope). Eumelanin and pheomelanin analyses were realized as described [26]. For tumors immunofluorescence, western blot and cell cycle analyses, mice were sacrificed between day one and day eight post-intravenously injection of 18.5 MBq [^{131}I]ICF01012. Tumors were excised and frozen in N_2 then stored at −80 °C for western blot analysis and cell cycle study as described [24], or fixed in 10% neutral buffered formalin (Sigma) and stored in 70% ethanol for immunofluorescence analysis.

Immunofluorescence

After deparaffinization and rehydration of the five μm-thick sections of B16BL6 tumors, antigen retrieval was conducted by incubating the slides in boiling antigen unmasking solution (Vector Laboratories) for 30 min. Endogenous peroxidase was quenched by incubation for 30 min in 0.3% H_2O_2, and non-specific sites were blocked with Antibody (Ab) diluent buffer (Dako) for 1 h at room temperature (RT). Slides were then incubated overnight (ON) at 4 °C in Ab dilution buffer with primary Ab. The following primary Abs were used: rabbit monoclonal anti-N-cadherin Ab (1/200) and rabbit monoclonal anti-vimentin Ab (1/200) both from Abcam. Isotype controls were slides incubated with irrelevant normal rabbit IgG (Sigma). Slides were washed twice with PBS, and incubated with fluorescence-

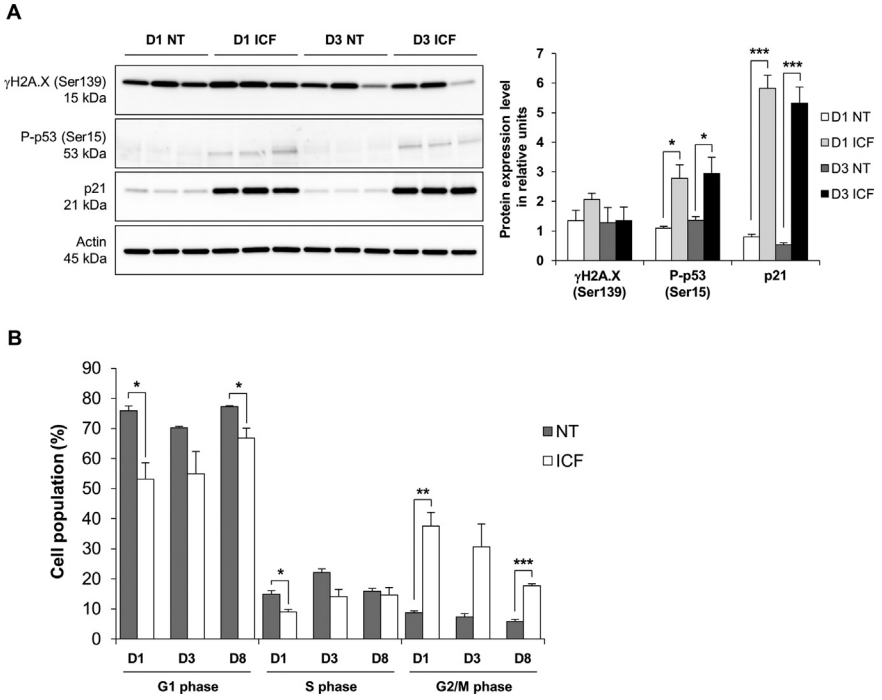

Figure 1. [131I]ICF01012 activates DNA damage responses and induces cell cycle arrest in B16BL6 *in vivo* **model.** (A) The expression of phospho-H2A.X (γH2A.X) Ser139, phospho-p53 (P-p53) Ser15 and p21 proteins were measured by western blot analysis in B16BL6 tumors excised from C57BL/6 J mice at day 1 (D1) and days 3 (D3) post-[131I]ICF01012 injection (n = 3 tumors per group). Actin was used as a loading protein control. The expression level was evaluated as the ratio of γH2A.X, P-p53 and p21 protein densities between non-treated tumors (NT) and [131I]ICF01012 treated tumors (ICF). $^{*}P < .05$; $^{***}P < .001$. (B) Cell cycle analysis of B16BL6 tumors excised at day 1 (D1), days 3 (D3) and day 8 (D8) post-[131I]ICF01012 injection (D1, D8 NT and ICF: n = 3 tumors per group; D3 ICF: n = 3 tumors per group, D3 NT: n = 2). Histograms mean % of cell population ± SD $^{*}P < .05$; $^{**}P < .01$, $^{***}P < .001$; when compared treated tumors (ICF) with their respective non-treated tumors (NT).

conjugated secondary Ab to rabbit IgG (1/500; Invitrogen) for 1 h at RT. Nuclei were stained with DAPI (0.1 μg/mL; Sigma). After slide mounting with Vectashield, emitting fluorescence was detected using Axio Imager 2 microscope (Zeiss), and analyzed with ZEN software (Zeiss).

Lung Histological Examination and Colonization Analysis

Fixed lungs were embedded in paraffin, sections of four μm thickness were realized and tissues were stained with hematoxylin-phloxin saffron (HPS). The morphology of tumor cells and adjacent tissue were then analyzed. After a two-dimensional lung surface reconstruction (NIS-Element software, Nikon), lung metastases areas were quantified with NIS-Analysis software (Nikon).

Spheroid Culture and [131I]ICF01012 Irradiation Protocol

To generate melanoma cell spheroids, cells were seeded at a density of 1000 cells/well, in 96-well non-adherent plates (ThermoFisher), with a final volume of 100 μl/well of complete cell culture medium supplemented with 0.5% methylcellulose (Bio-techne). At day 6 of culture, each spheroid was irradiated with 37 kBq of [131I]ICF01012/100 μl of cell culture medium (without FCS) or with medium alone for control. After 1 h of incubation, the irradiation medium was removed and replaced by a complete medium supplemented with 0.5% methylcellulose. Spheroids were then incubated for a various periods of time ranging from 1 h to 72 h.

Uptake Analysis

One hour post-irradiation, medium was removed and spheroids were washed twice, in wells, with PBS. Spheroids were then taken in 100 μl of PBS and distributed at a rate of three spheroids/tube. Activity was measured by 1480 Wizard Gamma Counter (Perkin Elmer) during 1 minute (min) and was normalized to the blank.

Colony Forming Assay

Twenty-four hours post-irradiation, 60 spheroids/condition were collected and centrifuged. Supernatants were removed and spheroids were dissociated with 500 μl collagenase IV (0.2%; Sigma) during 30 min at 37 °C. Cells were re-suspended, counted and seeded in 6 well plates with a 2 mL final volume of complete culture medium. SK-MEL3 cells were seeded at 7200 cells/well, SK-MEL28 at 1200 cells/well, and B16BL6 and B16F10 at 400 cells/well. After 18 days of incubation for SK-MEL3, 10 days for SK-MEL28 and 8 days for both B16F10 and B16BL6 cells, medium was removed and colonies were rinsed once with PBS. Colonies were then fixed by methanol absolute during 3 min then revealed with 0.5% crystal violet solution. The counting of colonies was realized using the ImageJ software. Plating efficiency (PE) and survival fraction (SF) were determined as described [27].

RT-qPCR Analysis

SK-MEL-3 spheroids were collected at 1 h and 4 h post-[131I] ICF01012 irradiation (60 spheroids/time/condition), frozen in N_2

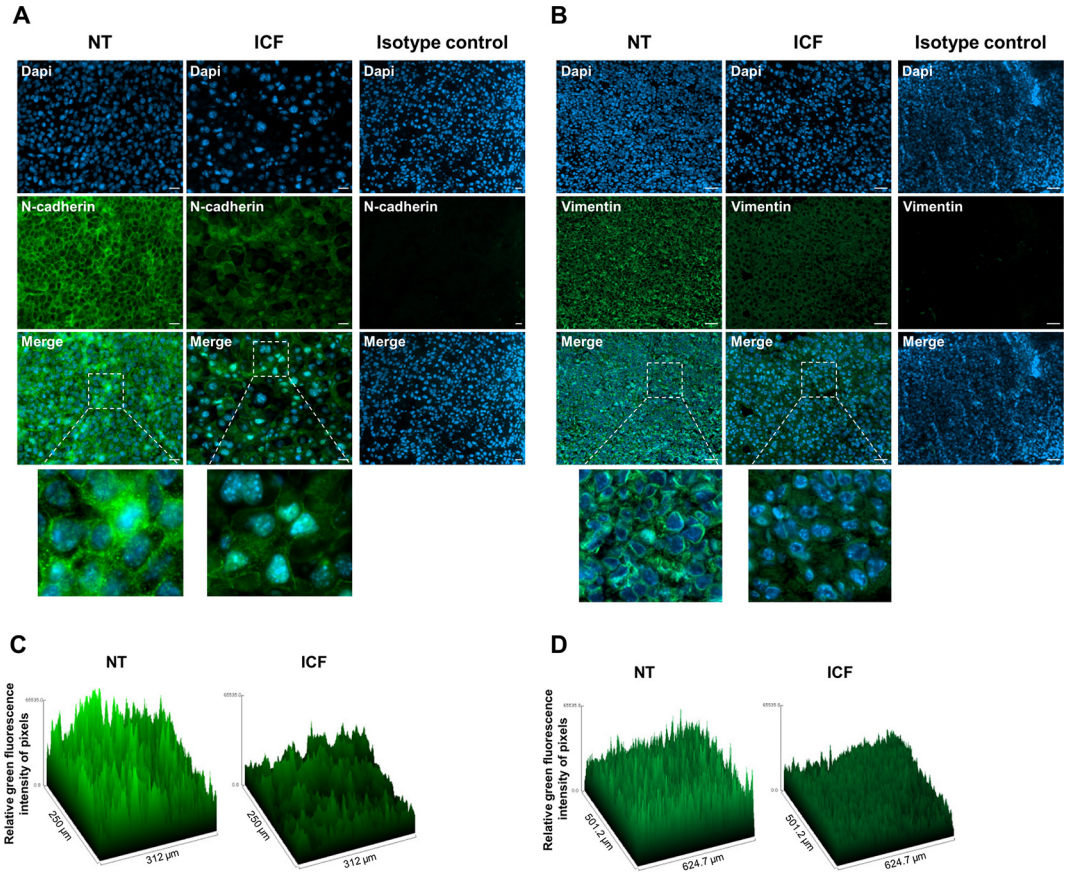

Figure 2. [^{131}I]ICF01012 decreases the expression of N-cadherin and vimentin in B16BL6 *in vivo* model. (A, B) Representative fluorescence immunohistochemistry analysis of N-cadherin and vimentin expressions in B16BL6 tumors excised from C57BL/6 J mice 3 days post-[^{131}I]ICF01012 injection (n = 3 tumors per group). Five μm-thick sections from non-treated (NT) and [^{131}I]ICF01012 treated tumors (ICF) were stained with anti-N-cadherin rabbit mAb (A) or anti-vimentin rabbit mAb (B) and revealed with Alexa fluor-488 conjugated fluorescent secondary antibodies (green). Nuclei were counterstained with DAPI (blue). (C, D) Relative quantification of N-cadherin expression (C) and vimentin expression (D) assessed by green fluorescent surface plot analysis. N-cadherin: magnification, x40; scale bars, 20 μm. Vimentin: magnification x20; scale bars, 50 μm.

and stored at −80 °C. After complete radioactive decay, RNA extraction was performed (RNA Extraction Kit; Qiagen) and RNA amounts were measured by spectrophotometry (MultiskanGo, ThermoFisher). cDNA were synthesized from 100 ng of RNA using Thermoscript kit (Fisher Scientific). Two reactions of transcriptase reverse were realized by sample. Quantitative PCR (qPCR) reactions were realized with Master Mix SybrGreen using Applied BioSystems StepOne Plus device. Primers and conditions of annealing are described in Supplementary Table 1. Results are expressed according to ΔΔCT method after normalization by the GAPDH housekeeping gene. Two qPCR are realized for each transcriptase reverse reaction.

Western Blotting

Western blot analysis was carried out as described [28]. Briefly, after complete radioactive decay, tumor proteins were extracted with urea buffer using GentleMACS Dissociator (Miltenyi Biotec). Spheroid proteins were extracted with Cell lysis buffer (Cell Signaling Technology). Thirty µg of tumor proteins, 20 µg of murine spheroid proteins and 15 µg of human spheroid proteins were separated by SDS-PAGE then transferred to nitrocellulose membranes (BioRad). The following primary Abs were used: anti-phospho-H2A.X (S139) (1/2000), anti-phospho-p53 (Ser15) (1/1000), anti-MITF (1/1000) from Cell Signaling Technology, anti-p21 (1/1000; Santa Cruz Biotechnology), anti-N-cadherin (1/5000), anti-vimentin (1/4000) from Abcam, and anti-Actin (1/10000; Sigma).

Statistical Analyses

Statistical analyses were performed with XLStat software (Addinsoft, VA, USA) and StatView software (Abacus concepts) using Student's t test for animal experiments, RT-qPCR analysis, cell cycle analysis and a one-way analysis of variances (ANOVA) for *in vitro* experiments, pigmentation analysis.

Results

Effects of [^{131}I]ICF01012 on DNA Damage Response and Cell Cycle in B16BL6 Melanoma Murine Model

To validate the antitumor effect of [^{131}I]ICF01012, we first examined the expression of specific proteins involved in DNA damage response (γH2A.X; phospho-p53) and cell cycle control (p21) in tumors extracted 1 day and 3 days after irradiation. Consistent with

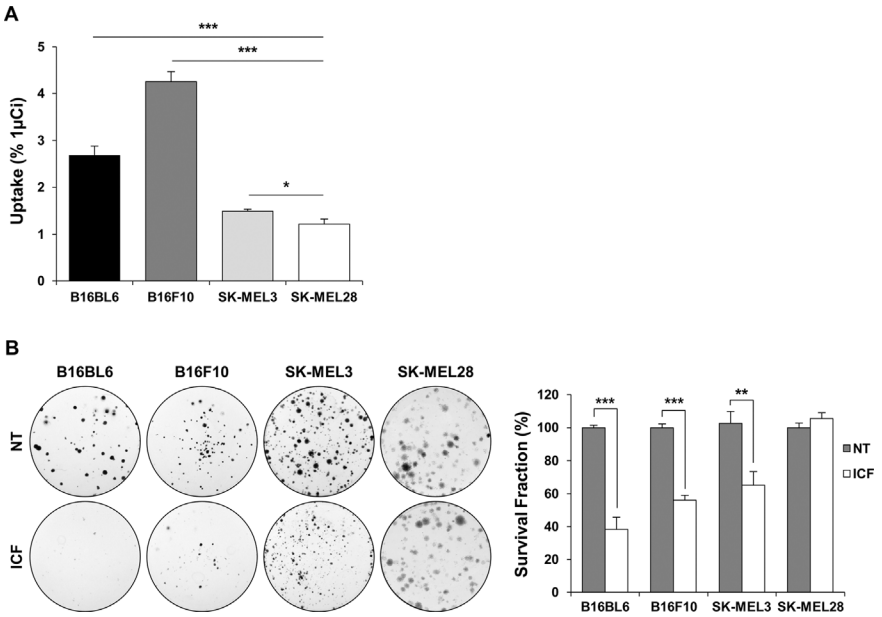

Figure 3. [^{131}I]ICF01012 reduces clonogenic capacity of melanoma spheroids in a cell pigmentation-dependent manner. (A) Uptake analysis of [^{131}I]ICF01012 in pigmented B16F10, B16BL6, SK-MEL3 and non-pigmented SK-MEL28 melanoma spheroids. Uptake analyses were realized after 1 h of spheroid incubation with [^{131}I]ICF01012. Histograms mean % of the uptake of the administrated dose (1 μCi) ± SEM of three independent experiments. *P < .05; ***P < .001; when compared with SK-MEL28 spheroids uptake. (B) Effect of [^{131}I]ICF01012 on clonogenic capacity of melanoma spheroids. Colony forming assays of B16BL6, B16F10, SK-MEL3 and SK-MEL28 melanoma spheroids 24 h post-[^{131}I]ICF01012 irradiation (ICF). Histograms mean % of survival fractions ± SEM of three independent experiments. *P < .05; ***P < .001; when compared with respective controls (NT).

our previous findings [24], [^{131}I]ICF01012 irradiation does not induce significant modifications on γH2A.X Serine 139 (Ser139) protein levels, after 1 day and 3 days of treatment (Figure 1*A*). However, it is worth mentioning that the basal γH2A.X expression level was high in the control tumors. In contrast, the expression level of phosphorylated p53 protein at Ser15 increased significantly in treated group compared to the non-treated group, after 1 day (1.7-fold increase) and 3 days (1.6-fold increase) post-irradiation (Figure 1*A*). The activation of p53 protein led to an increase of p21 protein expression, after 1 day (5-fold increase) and 3 days (4.8-fold increase) post-irradiation (Figure 1*A*). We subsequently analyzed cell cycle modifications in B16BL6 tumors after 1 day and 8 days post-[^{131}I]ICF01012 injection. In accordance with our previous studies [23,24], we showed that [^{131}I]ICF01012 significantly decreased the proportion of cells in G1 phase and induced G2/M phase arrest in these wild-type p53 B16BL6 tumor cells (Figure 1*B*).

[^{131}I]ICF01012 Alters the Expression of Epithelial-Mesenchymal Transition-Like Markers in B16BL6 Melanoma Murine Model

It is well known that EMT-like is an essential biological event for melanoma tumor invasion and metastasis. For that, we next investigated whether [^{131}I]ICF01012 treatment altered EMT-like in B16BL6 melanoma-bearing mice by immunohistochemical analysis. The expression of two EMT-like markers, the Neural cadherin (N-cadherin) and the vimentin, was assessed. Interestingly, 3 days post-irradiation, a reduction of mesenchymal N-cadherin (Figure 2, *A* and *C*) and vimentin (Figure 2, *B* and *D*) markers expression was observed when compared irradiated tumors to the non-treated tumors.

In Vitro Efficacy Study of [^{131}I]ICF01012 on Murine and Human Melanoma Tumor Spheroid Models

In order to study precisely the mechanisms underlying the effect of [^{131}I]ICF01012 treatment on invasion and antitumor efficacy, we established 3D *in vitro* spheroid models that mimic *in vivo* tumor mass architecture. First, we confirmed the uptake and the efficacy of [^{131}I]ICF01012 in murine (B16F10 and B16BL6) and in human melanoma spheroid models (SK-MEL3 and SK-MEL28). As shown in Figure 3*A*, the uptake of [^{131}I]ICF01012 is depending on cellular pigmentation in spheroids. Indeed, in comparison with the non-pigmented SK-MEL28 spheroids, [^{131}I]ICF01012 uptake is significantly higher in well pigmented murine spheroids (B16BL6 and B16F10) as well as in human less pigmented SK-MEL3 spheroids. The efficacy of [^{131}I]ICF01012 treatment where then determined using the clonogenic survival assay. Figure 3*B* demonstrates that [^{131}I]ICF01012 treatment reduces clonogenic capacity of all pigmented melanoma spheroids except for the non-pigmented SK-MEL28 spheroids. Compared to the non-treated spheroids, the survival fractions of irradiated spheroids were respectively 38.2% and 55.9% for both B16BL6 and B16F10 spheroids, 65.2% for SK-MEL3 spheroids and 105.6% for the non-pigmented SK-MEL28 spheroids.

Secondly, the effects of [^{131}I]ICF01012-induced DNA damage response and cell cycle arrest were determined using western blot analysis. Figure 4 shows that except for the non-pigmented SK-MEL28 spheroids, [^{131}I]ICF01012 induces DNA damage response

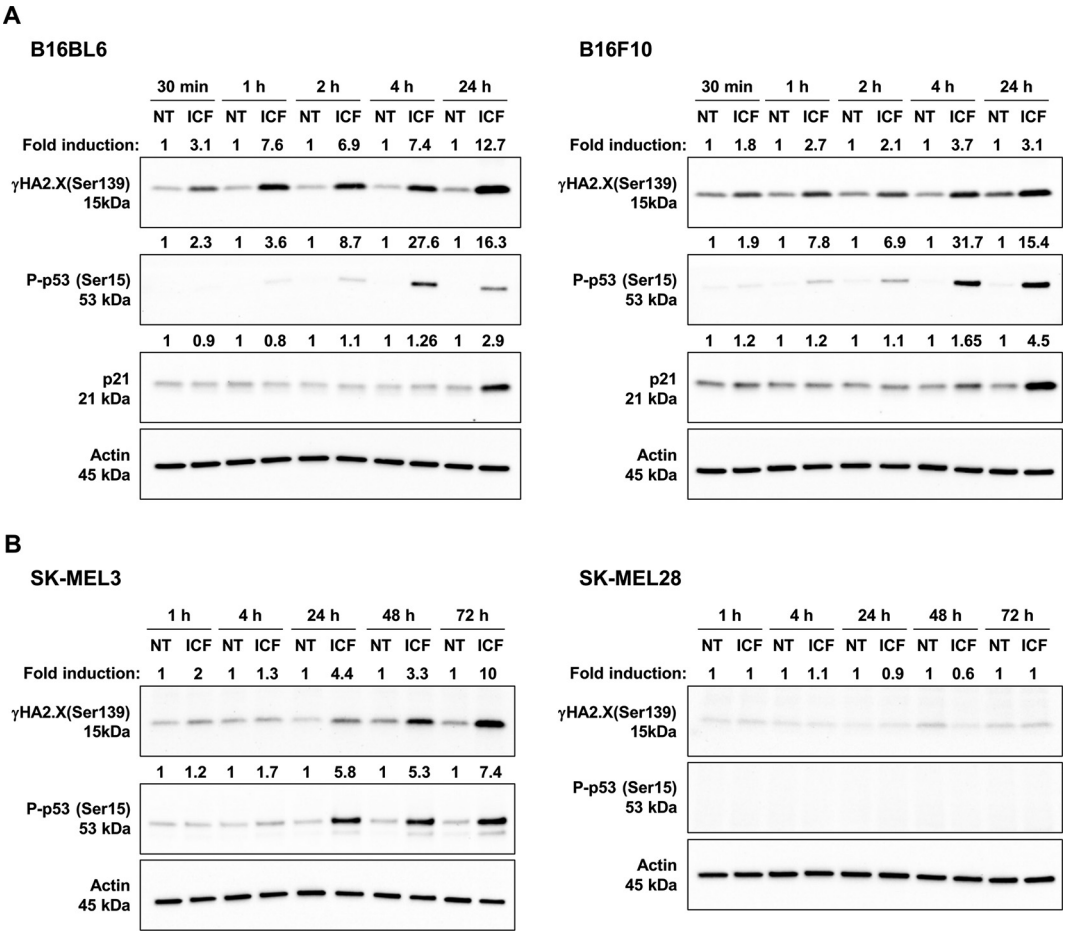

Figure 4. [^{131}I]ICF01012 activates DNA damage responses in pigmented melanoma spheroids. (A, B) The capacity of [^{131}I]ICF01012 to induce DNA damage signaling pathway in melanoma spheroids was assessed by western blot analysis using antibodies specific to γH2A.X (Ser139), P-p53 (Ser15) and p21 proteins. The pigmented murine B16BL6 and B16F10 spheroids (A), as well as the human pigmented SK-MEL3 and non-pigmented SK-MEL28 melanoma spheroids (B) were irradiated with [^{131}I]ICF01012 and harvested at indicated times. Actin was used as a loading protein control. The fold induction was evaluated as the ratio of γH2A.X, P-p53 and p21 protein densities between non-treated (NT) and [^{131}I]ICF01012 treated spheroids (ICF).

in all studied melanoma tumor spheroid models. The γH2A.X (Ser139) and phospho-p53 (P-p53) (Ser15) proteins expression levels were enhanced 30 min post-irradiation in the two murine B16BL6 (3.1-fold increase for γH2A.X and 2.3-fold increase for P-p53) as well as B16F10 (1.8-fold increase for γH2A.X and 1.9-fold increase for P-p53) spheroids, and remained higher than the controls up to 24 h (Figure 4*A*). [^{131}I]ICF01012 also increases the expression levels of these two DNA damage response markers, after 1 h of irradiation (2-fold increase for γH2A.X and 1.2-fold increase for P-p53) in SK-MEL3 human spheroids, and remained higher than the controls up to 72 h (Figure 4*B*). It is well known that p21 protein is an essential factor for the p53-mediated cell cycle arrest in cells with damaged DNA. As shown in Figure 4*A*, phosphorylation of p53 enhances the expression of p21 protein in wild-type p53 B16BL6 and B16F10 spheroids. The p21 protein was not detected in mutant p53 SK-MEL3 spheroids (data not shown). Taken together these data suggest that [^{131}I]ICF01012 mediates its antitumor effect by inducing DNA damage and cell cycle arrest coupled with reduced clonogenic capacity of pigmented melanoma spheroids.

[^{131}I]ICF01012 Reduces the Acquisition of EMT-Like Phenotype

To investigate the impact of [^{131}I]ICF01012 on spheroid models, EMT-like-related genes expression levels were measured in SK-MEL3 spheroids, using RT-qPCR analysis (Figure 5). Importantly, we showed an early 20% decrease of *SPARC* transcription 1 h post-irradiation. In addition, the expression levels of two *MITF* transcription regulatory factors, *BRN2* and *ZEB2*, were respectively decreased at 1 h (30% fold-decrease) and 4 h (15% fold-decreased) post-irradiation. Concomitantly, we observed a significant 15% *MITF* expression decrease. The other studied genes did not show significant transcription modification (Supplementary Figure 1). Western blot analysis of [^{131}I]ICF01012 treated spheroids afforded additional evidence to support [^{131}I]ICF01012-mediated reduction of EMT-like. Indeed, [^{131}I]ICF01012 decreases the expression levels of the two EMT-like markers N-cadherin and vimentin in, BRAF wild-type, B16BL6 and B16F10 murine spheroid models. The decreased expression levels of N-cadherin and vimentin were detected from 30 min post-irradiation in B16F10 spheroids (1.28 fold-decreased

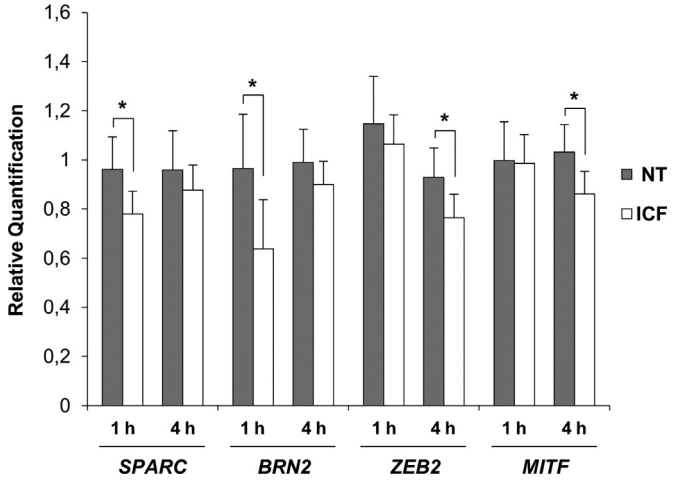

Figure 5. EMT-like-related genes expression in SK-MEL3 irradiated spheroids. RT-qPCR analysis of EMT-like-related genes expression in total RNA extracted from human melanoma SK-MEL3 spheroids at 1 h and 4 h post-[131I]ICF01012 irradiation. Target genes expression were normalized to the housekeeping GAPDH mRNA. The gene expression in treated spheroids (ICF) was compared to that of non-treated spheroids (NT) (fold-regulation). Results are presented as means Relative Quantification ± SEM of three independent experiments.*$P < .05$.

for N-cadherin and 1.5 fold-decreased for vimentin) and remained lower than the controls up to 24 h (Figure 6*A*). The same results were obtained for the B16BL6 spheroids (data not shown). [131I]ICF01012 irradiation of V600EBRAF-mutated SK-MEL3 spheroids appears to be less effective. Indeed, the expression levels of N-cadherin and vimentin proteins decreased slightly during the 48 h post-irradiation, then increased at 72 h (1.62 fold-increase for N-cadherin and 1.6 fold-increase for vimentin) suggesting a radioresistance sign of SK-MEL3 spheroids to the [131I]ICF01012-induced EMT-like reduction (Figure 6*B*). Although the specific role of MITF in EMT-like remains not fully understood, the relationship between the phenotype switching of melanoma cells and the level of MITF expression has been well reported. Indeed, it has been described that melanoma tumor cells with high MITF expression are differentiated and mostly proliferating cells, whereas those with low MITF expression are further invasive and less proliferating cells [29]. It is worth mentioning that [131I]ICF01012 decreases the expression of MITF at mRNA (Figure 5) and protein levels (Figure 6*C*) in SK-MEL3 spheroids confirming the radioresistance signs of these BRAF-mutant spheroids to [131I]ICF01012-mediated reduction of EMT-like.

[131I]ICF01012 Modifies Pigmentation

In order to investigate the effect of the [131I]ICF01012 treatment on melanogenesis, the expression of the tyrosinase protein was evaluated in human SK-MEL3 spheroids. Figure 7*A* shows that [131I]ICF01012 enhances the expression levels of the tyrosinase at 48 h and 72 h post-irradiation. Accordingly, we showed that [131I]ICF01012 treatment is accompanied by an increased level of total melanin from 5.8 to 8.4 μg/mg in SK-MEL-3 human xenografts (Figure 7*B*). Furthermore, eumelanin (Figure 7*C*) and pheomelanin (Figure 7*D*) were significantly increased with a constant ratio of pheomelanin/eumelanin (Figure 7*E*).

[131I]ICF01012 Decreases Lung Colonies in B16BL6 Melanoma Murine Model

We have previously shown that [131I]ICF01012 induced significant slowing of tumor growth and decreased spontaneous lung metastases in melanoma preclinical models [21,23,24,30]. To

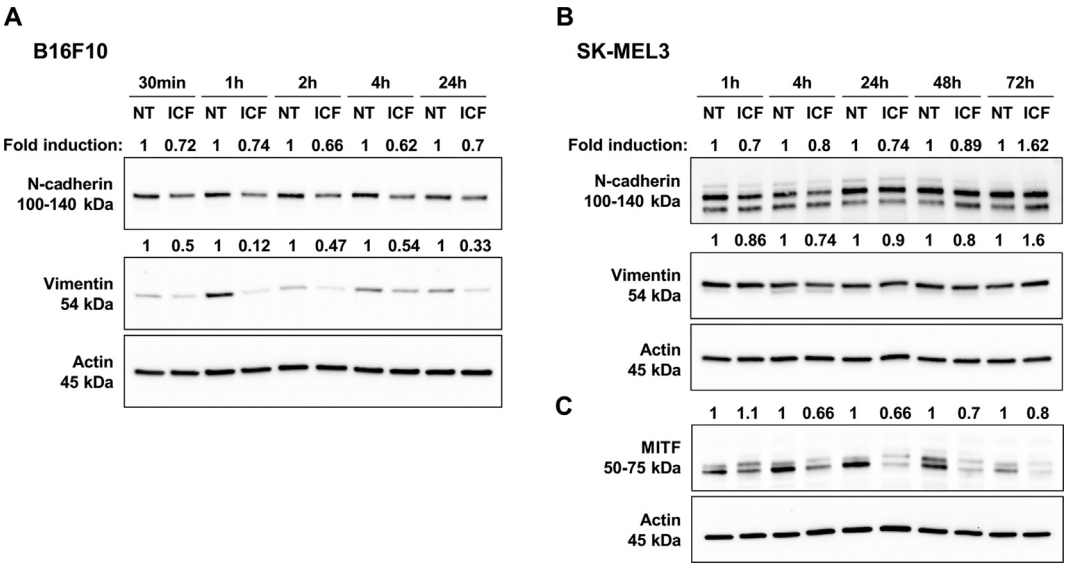

Figure 6. [131I]ICF01012 decreases the expression of EMT-like markers in melanoma spheroids. The expression of N-cadherin and vimentin were analyzed by western blot in total cellular protein extracted from B16F10 (A) and SK-MEL3 (B) spheroids that were treated (ICF) or not (NT) with [131I]ICF01012 and harvested at indicated times. Actin was used as a loading protein control. The fold induction was evaluated as the ratio of N-cadherin and vimentin protein densities between NT and ICF spheroids. (C) Western blot analysis of MITF in total cellular protein extracted from SK-MEL3 spheroids treated (ICF) or not (NT) with [131I]ICF01012 and harvested at indicated times. Actin was used as a loading protein control. The fold induction was evaluated as the ratio of MITF protein densities between NT and ICF spheroids.

assess the ability of [^{131}I]ICF01012 to destroy circulating tumor cells and to limit distant organ invasion, we examined here the efficiency of [^{131}I]ICF01012 on pigmented B16BL6 melanoma lung colonies. As shown in Figure 8, *A* and *B*, 13 days after intravenous injection of 18.75 MBq [^{131}I]ICF01012, a significant decrease of lung weight between control and treated groups (257 ± 59 *vs* 174 ± 41 mg, respectively) was observed. To consolidate this result, a quantification of metastasis areas was performed on random HPS lung slices (Figure 8, *C–E*). In control group, the median of the lung invasion was 12.65%. [^{131}I]ICF01012-TRT decreased significantly the size of metastases and the median of invasion did not exceed 1% of the lung surface (*i.e.* 0.75%; Figure 8*D*). Lung colonies-adjacent tissue was evaluated and no macroscopic changes were observed after [^{131}I]ICF01012 treatment.

Discussion

The functional consequences of radiotherapy on tumor aggressiveness remain a matter of debate, with results from preclinical models being different to those observed in clinical studies. Indeed, EBRT was often associated with an enhancement of metastatic processes in experimental *in vitro* and *in vivo* studies, while the effects of EBRT on patients are associated with favorable survival without progression [25]. In this study, we addressed some questions about the impact of TRT on invasion and metastatic dissemination processes. We have previously reported a regression of spontaneous melanoma metastases in B16BL6 model [21]. Here we observed a decrease of melanoma lung colonies, after intravenous injection of cells, following TRT. Taken together these findings suggest that [^{131}I]ICF01012 modifies metastatic processes presumably by the reduction of angiogenesis, cell motility and invasion. We indeed showed a decrease of vascular endothelial growth factor as well as of small vessels in irradiated tumors [23]. The reduction of metastatic invasion induced by [^{131}I]ICF01012 should be related to EMT-like; indeed the expression of N-cadherin and vimentin, two proteins involved in the EMT, were reduced in tumors after [^{131}I]ICF01012 treatment. Besides, we demonstrated that [^{131}I]ICF01012, by remaining a long time in the tumor, induces a sustained DNA damage response and cell cycle blockade as evidenced by the G2/M arrest and the increased amount of phosphorylated p53 protein and its downstream target p21 protein. [^{131}I]ICF01012 seemed also able to modify the second part of metastatic process, which is the homing of circulating cells to target tissues. Our findings indeed showed a significant decrease of lung colonies, suggesting that [^{131}I]ICF01012 can kill circulating pigmented melanoma cells and/or modify their program to reduce their extravasation and proliferation in lungs.

In order to investigate specifically the effect of [^{131}I]ICF01012 on melanoma metastasizing capacity, we developed 3D cell culture models and demonstrated their relevance for TRT study. We showed that [^{131}I]ICF01012 can penetrate spheroids in a cell pigmentation-dependent manner and provokes DNA damage and cell cycle arrest, only in pigmented ones. These findings were in line with *in vivo* results [30] and validated spheroids to further explore TRT-induced mechanisms. Indeed, in the murine BRAF wild-type B16BL6 and B16F10 melanoma spheroids, we showed an early and continuous decrease of EMT-like markers, post-TRT treatment. In the human ^{V600E}BRAF-mutant SK-MEL3 spheroids, TRT-induced EMT-like reduction was less pronounced. SK-MEL3 cells are derived from a metastatic lymph node and we can assume that these cells are in an invasive state. Indeed, at the mRNA level, [^{131}I]ICF01012 induced an early and transitory decrease of *SPARC* transcription, a coding gene for a secreted extracellular matrix-associated protein that is involved in the EMT-like, by facilitating melanoma cell spreading specifically to the lung [31]. [^{131}I]ICF01012 treatment also transiently modified the expression level of *MITF* and its transcription activator *ZEB2*. MITF is a key transcription factor involved in proliferation and invasion of melanoma cells. Its regulation obeys to a complex rheostat: an MITF^{low}/ ZEB2^{low} expression favors invasion, characteristic of a mesenchymal state, and an MITF^{high}/ ZEB2^{high} expression favors proliferation and differentiation, characteristics of an epithelial state [32]. Besides, MITF expression levels are precisely regulated in melanoma cells to ensure their survival, because a very low level of MITF expression leads to cell death and a too high level induces cell cycle arrest and differentiation [33]. Additionally, Wellbrock et al. [33] have shown that proliferation in ^{V600E}BRAF melanoma cells is regulated through the activation of MITF promoter by the oncogenic ^{V600E}BRAF/ERK/BRN2 pathway with a MITF-BRN2 reciprocal repression. In the ^{V600E}BRAF spheroids, 4 h post-irradiation, [^{131}I]ICF01012 treatment of SK-MEL3 spheroids resulted in a transient decrease in MITF mRNA expression as well as its transcriptional activator ZEB2, suggesting a form of radioresistance through an increase of invasiveness, according to Caramel et al. [32]. But, the early reduction of BRN2 (1 h after treatment) precedes MITF expression decrease and could be interpreted as a limitation of invasion and support the idea of cell death induced by a very low MITF expression in the early time following treatment in this ^{V600E}BRAF model. On the other hand, we did not find significant transcription modifications for other EMT-like markers as E-cadherin (epithelial state) or N-cadherin (mesenchymal state), neither for stemness genes as *OCT4*, proliferation genes as *PCNA,* or for genes involved in differentiation as tyrosinase (*TYR*). Nevertheless, in the same model, we described a first slight decrease of N-cadherin and vimentin protein expressions followed however by an increase at 72 h post-irradiation. These results suggest a post-translational impact of [^{131}I]ICF01012 and an initial decrease of EMT-like followed by a form of radioresistance in these BRAF-mutant spheroids. We also observed an early decrease of MITF protein at 4 h post-irradiation, confirming the RT-qPCR results, followed however by an increase of tyrosinase protein expression, which suggests an enhancement of cell differentiation. Accordingly, we showed that [^{131}I]ICF01012 increases pigmentation in human SK-MEL3 xenograft model, confirming the hypothesis of differentiation induction in the human BRAF-mutant melanoma cells after [^{131}I]ICF01012 treatment. Despite the specificity of [^{131}I]ICF01012 for pigmented melanoma and the inefficacy of [^{131}I]ICF01012 on non-pigmented M3Dau melanoma xenografts [20], the property of this TRT to induce melanin synthesis should contribute to cure poorly pigmented lesions. An interesting point will be to assess the effect of TRT on mixed metastatic lesions *i.e.* pigmented and non-pigmented ones and to observe if an abscopal effect will occur.

Conclusions

We provide here additional proof on the pertinence of [^{131}I]ICF01012-TRT approach for pigmented metastatic melanoma. We thus demonstrated that [^{131}I]ICF01012 reduces tumor metastatic capacity by modifying the expression of EMT-like markers. We also proved the relevance of a spheroid model for this type of study. However, the precise regulation remains unclear. In B16 mouse

melanoma model, [131I]ICF01012 decreases the expression of the EMT-like main proteins N-cadherin and vimentin. In human melanoma V600EBRAF model, the effects of [131I]ICF01012 are more puzzling: there are arguments for an early efficiency associated with a differentiation (pigmentation) but the question of an induction of radioresistance arises. The increase of pigmentation can also be assimilated to a defense mechanism against the radiation, which could be beneficial in the hypothesis of a repeated treatment. Further

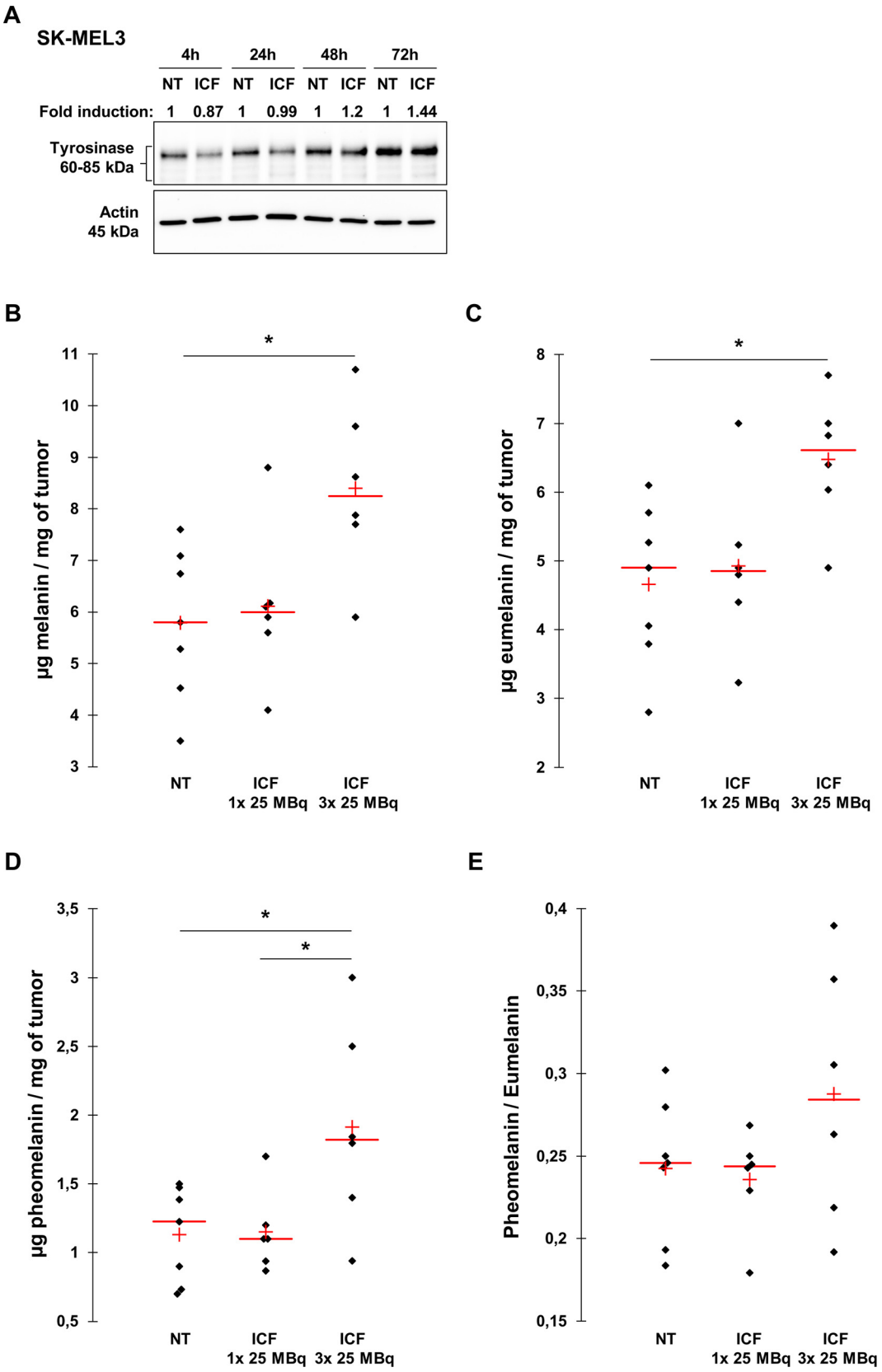

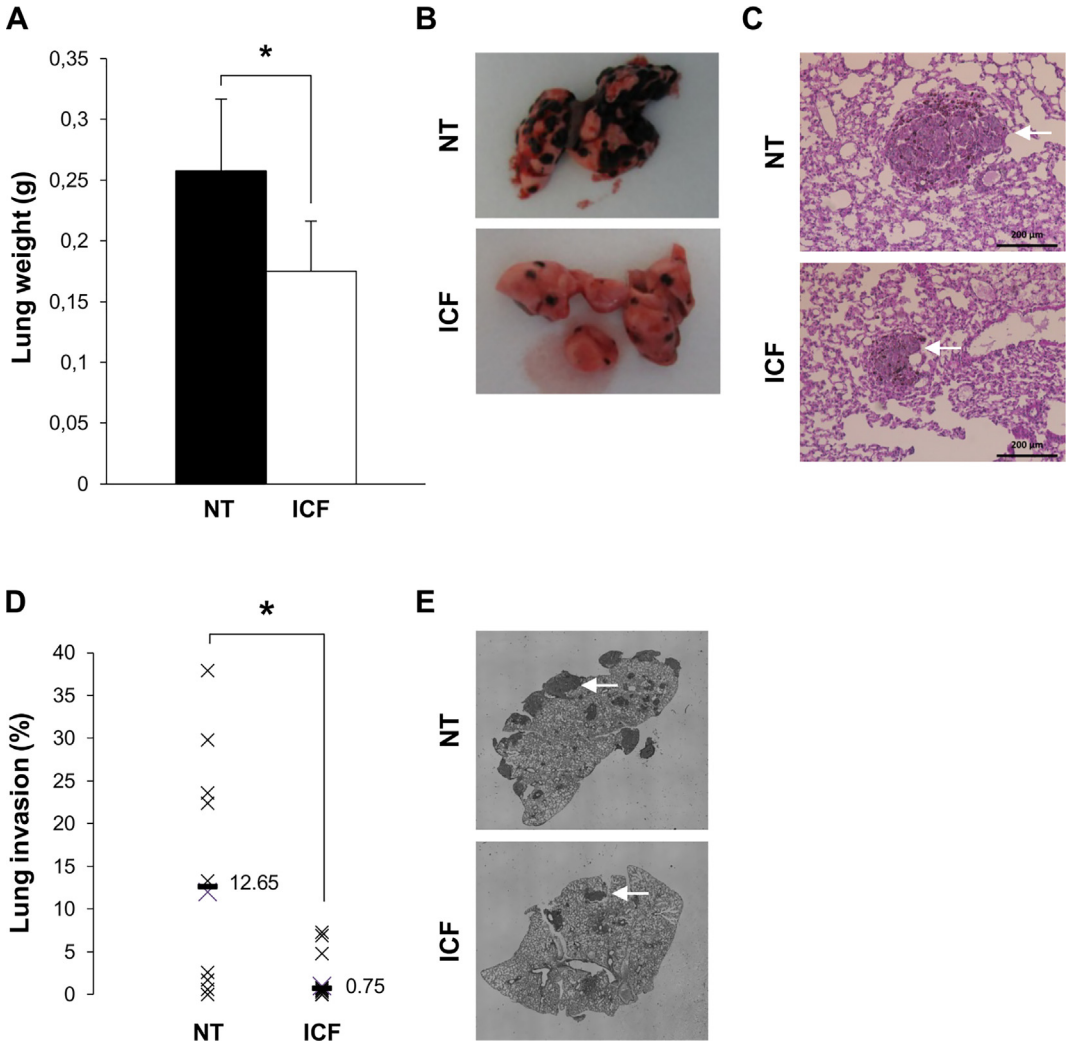

Figure 8. [^{131}I]ICF01012 reduces lung colonization in B16BL6 syngeneic model. C57BL/6 J mice were injected intravenously into the tail vein with 1.5 × 10^5 B16BL6 melanoma cells to induce lung colonies. After 7 days, mice were non-treated (NT) or received an intravenous injection of 18.5 MBq [^{131}I]ICF01012 (ICF) (n = 10 mice per group). Mice were sacrificed on day 13 post-[^{131}I]ICF01012 injection and lungs were excised and weighed. (A) Histograms mean lungs weight from each group ± SD *P < .05. (B) Representative images of lungs from each group. (C) Representative HPS histological stained sections of lungs from each group (nodules are indicated by arrows; Scale bars, 200 μm). (D) Scattergram representing the percentage of B16BL6 lung invasion from each group. *P < .05. (E) Representative two-dimensional reconstructions of lungs surface from each group (nodules are indicated by arrows).

investigations, in syngeneic spontaneous melanoma model or in patients-derived xenografts, are mandatory to better understand the precise mechanisms that underlie the effects of [^{131}I]ICF01012-TRT.

Supplementary data to this article can be found online at https://doi.org/10.1016/j.tranon.2019.07.015.

Acknowledgments

We are grateful to Dr. M. Bonnet (UMR 1071, Clermont-Ferrand) for her expertise concerning RT-qPCR analyses. We also thank Master's students, Raphael Benalouane and Zenthao Shao, for their participation to this project. We want to acknowledge the anatomopathology department of the Centre Jean Perrin and the CICS for the immunofluorescence and flow cytometry studies.

Conflict of interest

The authors have no conflict of interest to declare.

Figure 7. [^{131}I]ICF01012 enhances melanoma cell pigmentation. (A) Western blot analysis of tyrosinase expression for SK-MEL3 spheroids treated (ICF) or not (NT) with [^{131}I]ICF01012 and harvested at indicated times. Actin was used as a loading protein control. The fold induction was evaluated as the ratio of tyrosinase protein densities between NT and ICF spheroids. (B) Spectrophotometry analysis of total melanin content in SK-MEL3 xenograft model. Data are represented as a scattergram of melanin content in μg/mg of tumor (n = 7 tumors per group). Total melanin content was measured in tumors excised from Swiss nu/nu mice that were either NT or treated once intravenously with 25 MBq of [^{131}I]ICF01012 (ICF 1× 25 MBq) or thrice (once-weekly) (ICF 3× 25 MBq). *P < .05. (C, D) Quantitative analysis of eumelanin and pheomelanin contents in SK-MEL3 xenograft tumors. Data are represented as scattergrams of eumelanin (C) and pheomelanin (D) contents in μg/mg of tumors (n = 7 tumors per group) from the three SK-MEL3 xenograft tumors groups. *P < .05. (E) Scattergram of pheomelanin/eumelanin ratios, in relative units, of the three SK-MEL3 xenograft tumors groups.

References

[1] Siegel RL, Miller KD, and Jemal A (2019). Cancer statistics, 2019. *CA Cancer J Clin* **69**, 7–34.

[2] Pearlman RL, Montes de Oca MK, Pal HC, and Afaq F (2017). Potential therapeutic targets of epithelial-mesenchymal transition in melanoma. *Cancer Lett* **391**, 125–140.

[3] Larkin J, Ascierto PA, Dreno B, Atkinson V, Liszkay G, Maio M, Mandala M, Demidov L, Stroyakovskiy D, and Thomas L, et al (2014). Combined vemurafenib and cobimetinib in BRAF-mutated melanoma. *N Engl J Med* **371**, 1867–1876.

[4] Larkin J, Hodi FS, and Wolchok JD (2015). Combined Nivolumab and Ipilimumab or Monotherapy in Untreated Melanoma. *N Engl J Med* **373**, 1270–1271.

[5] Flaherty KT, Puzanov I, Kim KB, Ribas A, McArthur GA, Sosman JA, O'Dwyer PJ, Lee RJ, Grippo JF, and Nolop K, et al (2010). Inhibition of mutated, activated BRAF in metastatic melanoma. *N Engl J Med* **363**, 809–819.

[6] Johnson DB, Sullivan RJ, Ott PA, Carlino MS, Khushalani NI, Ye F, Guminski A, Puzanov I, Lawrence DP, and Buchbinder EI, et al (2016). Ipilimumab Therapy in Patients With Advanced Melanoma and Preexisting Autoimmune Disorders. *JAMA Oncol* **2**, 234–240.

[7] Fonkem E, Uhlmann EJ, Floyd SR, Mahadevan A, Kasper E, Eton O, and Wong ET (2012). Melanoma brain metastasis: overview of current management and emerging targeted therapies. *Expert Rev Neurother* **12**, 1207–1215.

[8] Khan N, Khan MK, Almasan A, Singh AD, and Macklis R (2011). The evolving role of radiation therapy in the management of malignant melanoma. *Int J Radiat Oncol Biol Phys* **80**, 645–654.

[9] Hearing VJ (2000). The melanosome: the perfect model for cellular responses to the environment. *Pigment Cell Res* **13**(Suppl 8), 23–34.

[10] Cichorek M, Wachulska M, Stasiewicz A, and Tyminska A (2013). Skin melanocytes: biology and development. *Postepy Dermatol Alergol* , **30**, 30–41.

[11] Delevoye C (2014). Melanin transfer: the keratinocytes are more than gluttons. *J Invest Dermatol* **134**, 877–879.

[12] Svensson SP, Lindgren S, Powell W, and Green H (2003). Melanin inhibits cytotoxic effects of doxorubicin and daunorubicin in MOLT 4 cells. *Pigment Cell Res* **16**, 351–354.

[13] Dadachova E and Casadevall A (2005). Melanin as a potential target for radionuclide therapy of metastatic melanoma. *Future Oncol* **1**, 541–549.

[14] Cachin F, Miot-Noirault E, Gillet B, Isnardi V, Labeille B, Payoux P, Meyer N, Cammilleri S, Gaudy C, and Razzouk-Cadet M, et al (2014). (123)I-BZA2 as a melanin-targeted radiotracer for the identification of melanoma metastases: results and perspectives of a multicenter phase III clinical trial. *J Nucl Med* **55**, 15–22.

[15] Norain A and Dadachova E (2016). Targeted radionuclide therapy of melanoma. *Semin Nucl Med* **46**, 250–259.

[16] Klein M, Lotem M, Peretz T, Zwas ST, Mizrachi S, Liberman Y, Chisin R, Schachter J, Ron IG, and Iosilevsky G, et al (2013). Safety and efficacy of 188-rhenium-labeled antibody to melanin in patients with metastatic melanoma. *J Skin Cancer* **2013**828329.

[17] Miao Y, Shelton T, and Quinn TP (2007). Therapeutic efficacy of a 177Lu-labeled DOTA conjugated alpha-melanocyte-stimulating hormone peptide in a murine melanoma-bearing mouse model. *Cancer Biother Radiopharm* **22**, 333–341.

[18] Moins N, D'Incan M, Bonafous J, Bacin F, Labarre P, Moreau MF, Mestas D, Noirault E, Chossat F, and Berthommier E, et al (2002). 123I-N-(2-diethylaminoethyl)-2-iodobenzamide: a potential imaging agent for cutaneous melanoma staging. *Eur J Nucl Med Mol Imaging* **29**, 1478–1484.

[19] Mier W, Kratochwil C, Hassel JC, Giesel FL, Beijer B, Babich JW, Friebe M, Eisenhut M, Enk A, and Haberkorn U (2014). Radiopharmaceutical therapy of patients with metastasized melanoma with the melanin-binding benzamide 131I-BA52. *J Nucl Med* **55**, 9–14.

[20] Bonnet M, Mishellany F, Papon J, Cayre A, Penault-Llorca F, Madelmont JC, Miot-Noirault E, Chezal JM, and Moins N (2010). Anti-melanoma efficacy of internal radionuclide therapy in relation to melanin target distribution. *Pigment Cell Melanoma Res* **23**, e1–11.

[21] Bonnet-Duquennoy M, Papon J, Mishellany F, Labarre P, Guerquin-Kern JL, Wu TD, Gardette M, Maublant J, Penault-Llorca F, and Miot-Noirault E, et al (2009). Targeted radionuclide therapy of melanoma: anti-tumoural efficacy studies of a new 131I labelled potential agent. *Int J Cancer* **125**, 708–716.

[22] Chezal JM, Papon J, Labarre P, Lartigue C, Galmier MJ, Decombat C, Chavignon O, Maublant J, Teulade JC, and Madelmont JC, et al (2008). Evaluation of radiolabeled (hetero)aromatic analogues of N-(2-diethylaminoethyl)-4-iodobenzamide for imaging and targeted radionuclide therapy of melanoma. *J Med Chem* **51**, 3133–3144.

[23] Degoul F, Borel M, Jacquemot N, Besse S, Communal Y, Mishellany F, Papon J, Penault-Llorca F, Donnarieix D, and Doly M, et al (2013). In vivo efficacy of melanoma internal radionuclide therapy with a 131I-labelled melanin-targeting heteroarylcarboxamide molecule. *Int J Cancer* **133**, 1042–1053.

[24] Viallard C, Chezal JM, Mishellany F, Ranchon-Cole I, Pereira B, Herbette A, Besse S, Boudhraa Z, Jacquemot N, and Cayre A, et al (2016). Targeting DNA repair by coDbait enhances melanoma targeted radionuclide therapy. *Oncotarget* **7**, 12927–12936.

[25] Sundahl N, Duprez F, Ost P, De Neve W, and Mareel M (2018). Effects of radiation on the metastatic process. *Mol Med* **24**, 16.

[26] Rioux B, Rouanet J, Akil H, Besse S, Debiton E, Bouchon B, Degoul F, and Quintana M (2019). Determination of eumelanin and pheomelanin in melanomas using solid-phase extraction and high performance liquid chromatography-diode array detection (HPLC-DAD) analysis. *J Chromatogr B Analyt Technol Biomed Life Sci* **1113**, 60–68.

[27] Buch K, Peters T, Nawroth T, Sanger M, Schmidberger H, and Langguth P (2012). Determination of cell survival after irradiation via clonogenic assay versus multiple MTT Assay–a comparative study. *Radiat Oncol* **7**(1).

[28] Akil H, Abbaci A, Lalloue F, Bessette B, Costes LM, Domballe L, Charreau S, Guilloteau K, Karayan-Tapon L, and Bernard FX, et al (2015). IL22/IL-22R pathway induces cell survival in human glioblastoma cells. *PLoS One* **10**e0119872.

[29] Seberg HE, Van Otterloo E, and Cornell RA (2017). Beyond MITF: Multiple transcription factors directly regulate the cellular phenotype in melanocytes and melanoma. *Pigment Cell Melanoma Res* **30**, 454–466.

[30] Viallard C, Perrot Y, Boudhraa Z, Jouberton E, Miot-Noirault E, Bonnet M, Besse S, Mishellany F, Cayre A, Maigne L, et al. (2015). [(1)(2)(3)I]ICF01012 melanoma imaging and [(1)(3)(1)I]ICF01012 dosimetry allow adapted internal targeted radiotherapy in preclinical melanoma models *Eur J Dermatol* **25**, 29-35.

[31] Botti G, Scognamiglio G, Marra L, Collina F, Di Bonito M, Cerrone M, Grilli B, Anniciello A, Franco R, and Fulciniti F, et al (2014). SPARC/osteonectin is involved in metastatic process to the lung during melanoma progression. *Virchows Arch* **465**, 331–338.

[32] Caramel J, Papadogeorgakis E, Hill L, Browne GJ, Richard G, Wierinckx A, Saldanha G, Osborne J, Hutchinson P, and Tse G, et al (2013). A switch in the expression of embryonic EMT-inducers drives the development of malignant melanoma. *Cancer Cell* **24**, 466–480.

[33] Wellbrock C, Rana S, Paterson H, Pickersgill H, Brummelkamp T, and Marais R (2008). Oncogenic BRAF regulates melanoma proliferation through the lineage specific factor MITF. *PLoS One* **3**e2734.